U.S. DEPARTMENT OF ENERGY

PNNL-19767

Prepared for the U.S. Department of Energy
under Contract DE-AC05-76RL01830

Chemical Species in the Vapor Phase of Hanford Double-Shell Tanks:

Potential Impacts on Waste Tank Corrosion Processes

Andrew R. Felmy
Odeta Qafoku
Bruce Arey
Kayle D. Boomer

September 2010

Pacific Northwest
NATIONAL LABORATORY

Proudly Operated by Battelle *Since 1965*

DISCLAIMER

PACIFIC NORTHWEST NATIONAL LABORATORY
operated by
BATTELLE
for the
UNITED STATES DEPARTMENT OF ENERGY
under Contract DE-AC05-76RL01830

Printed in the United States of America

Available to DOE and DOE contractors from the
Office of Scientific and Technical Information,
P.O. Box 62, Oak Ridge, TN 37831-0062;
ph: (865) 576-8401
fax: (865) 576-5728
email: reports@adonis.osti.gov

Available to the public from the National Technical Information Service,
U.S. Department of Commerce, 5285 Port Royal Rd., Springfield, VA 22161
ph: (800) 553-6847
fax: (703) 605-6900
email: orders@ntis.fedworld.gov
online ordering: http://www.ntis.gov/ordering.htm

This document was printed on recycled paper.
(9/2003)

PNNL-19767

Chemical Species in the Vapor Phase of Hanford Double-Shell Tanks:

Potential Impacts on Waste Tank Corrosion Processes

AR Felmy
O Qafoku
B Arey
KD Boomer

September 2010

Prepared for the U.S. Department of Energy
under Contract DE-AC05-76RL01830

Pacific Northwest National Laboratory
Richland, Washington 99352

Introduction

The presence of corrosive and inhibiting chemicals on the tank walls in the vapor space, arising from the waste supernatant, dictate the type and degree of corrosion that occurs there. An understanding of how waste chemicals are transported to the walls and the affect on vapor species from changing supernatant chemistry (e.g., pH, etc.), are basic to the evaluation of risks and impacts of waste changes on vapor space corrosion (VSC).

In order to address these issues the expert panel workshop on double-shell tank (DST) vapor space corrosion testing (RPP-RPT-31129) participants made several recommendations on the future data and modeling needs in the area of DST corrosion. In particular, the drying of vapor phase condensates or supernatants can form salt or other deposits at the carbon steel interface resulting in a chemical composition at the near surface substantially different from that observed directly in the condensates or the supernatants. As a result, over the past three years chemical modeling and experimental studies have been performed on DST supernatants and condensates to predict the changes in chemical composition that might occur as condensates or supernatants equilibrate with the vapor space species and dry at the carbon steel surface. The experimental studies included research on both the chemical changes that occurred as the supernatants dried as well as research on how these chemical changes impact the corrosion of tank steels. The chemical modeling and associated experimental studies were performed at the Pacific Northwest National Laboratory (PNNL) and the research on tank steel corrosion at the Savannah River National Laboratory (SRNL).

This report presents a summary of the research conducted at PNNL with special emphasis on the most recent studies conducted in FY10. An overall summary of the project results as well as their broader implications for vapor space corrosion of the DST's is given at the end of this report.

Phase 1: Literature Review of vapor phase species in the DST's.

This overall project was initiated in FY2007 with an extensive literature review of the available data on vapor phase species compositions and associated supernatant compositions. CO_2 and NH_3 were found to be the major vapor phase species impacting the pH and chemical composition of possible vapor condensates. The CO_2 and NH_3 concentrations were found to vary widely with potentially large impacts on the pH of condensates or other solutions exposed on the tank walls. Organic analysis of the tank vapors showed a wide range of organic compounds most of which were at relatively low total concentration (<0.1ppm). The major organic species found in the vapors were methanol, ethanol and 1-butanol. 1-butanol originating from the disposal of the complexing agent tributylphosphate. In addition to the data for the vapor phase species, a summary of the data available for vapor phase condensates, from the AZ-702 ventilation system was also included. These analyses show a chemical system dominated by ammonium nitrate. The source of ammonia was from the vapor phase while the source of the nitrate was uncertain but believed to originate from the formation of nitric acid via the radiolysis of nitrogen gas in the headspace. No evidence was found for the importance of aerosols in impacting the chemical composition of the condensates since the four waste tanks in the AZ-702 ventilation system all had high nitrite/nitrate ratios (see Figure 1) whereas the condensates showed the opposite effect in having higher nitrate/nitrite ratios. This fact coupled with the differences in dominant cation (i.e. ammonium in the condensate and sodium in the supernatant) was a strong indication of a lack importance of aerosols in determining condensate chemistry. The presence of small concentrations of Na does indicate that aerosols could have been present, but their concentration was too low to impact the overall chemistry of the condensates in these samples. Felmy and Qafoku (2007) gives a complete summary of this research.

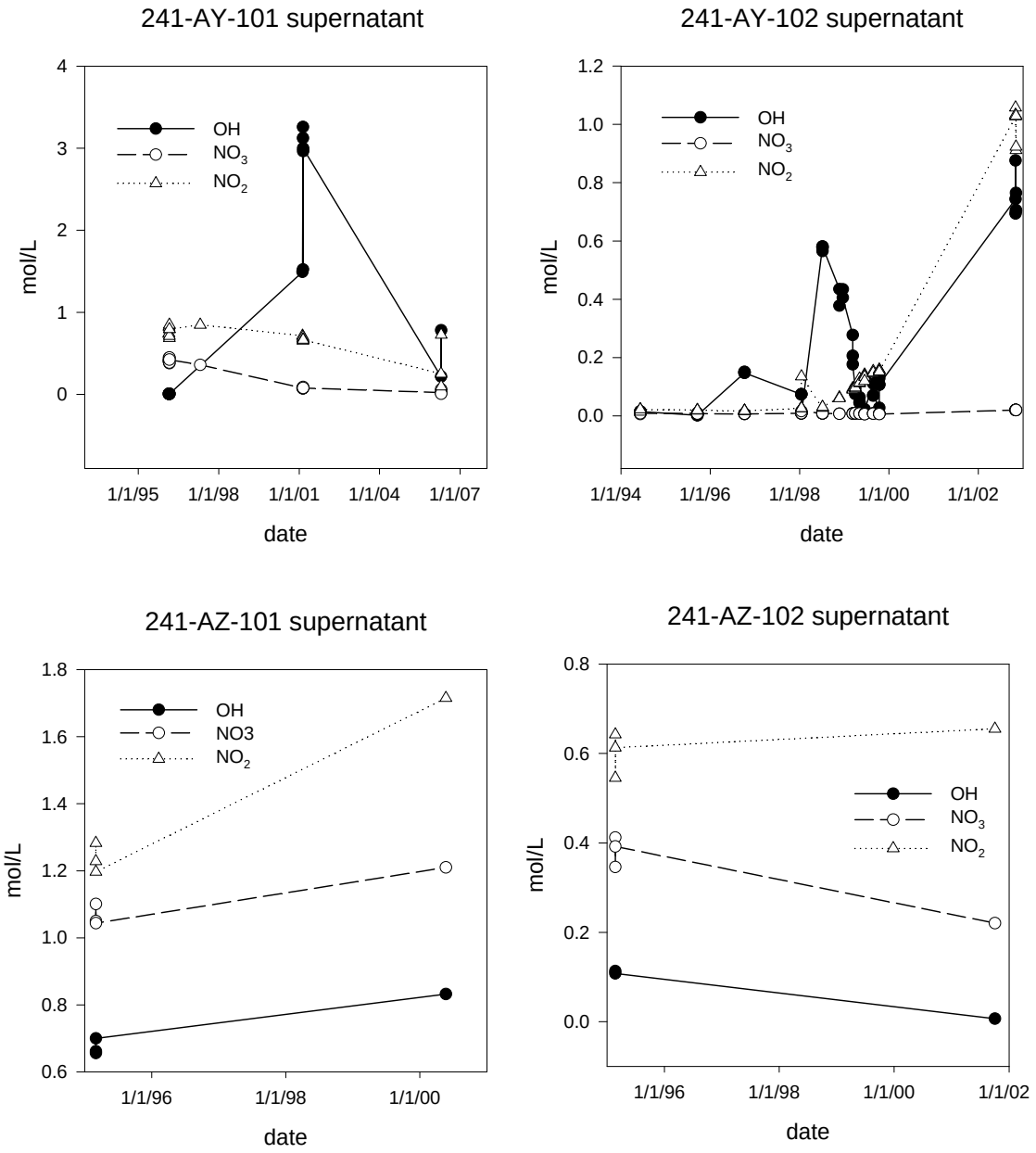

Figure 1. Nitrite and nitrate concentrations for supernatants found in the AZ-702 ventilation system (from Felmy and Qafoku 2007).

Phase 2: Thermodynamic Modeling

During phase two of this study (FY2008) the thermodynamic models were acquired and the data bases updated with more recent literature data. The thermodynamic models predicted that during the evaporation or drying processes of condensates their pH should remain relatively stable until the solutions were almost completely dessicated and solid precipitation occurs. The pH changes that take place during this final drying step depend upon the initial pH, the formation of unusual species (carbamates) and the predicted solids (Figure 2). The results also show that the initial condensate pH should be maintained above 9 to prevent rapid pH decreases during the later stages of drying. This will require the CO_2 be maintained below 80ppm and ammonia above 40ppm. It was

recommended that an experimental program be initiated to test/verify these results. The pH of supernatants at the liquid/air interface (LAI) can be significantly impacted by changes in CO_2 but not ammonia since the pH values for the tanks examined never dropped below 10 over the range of CO_2 concentrations observed. Felmy and Qafoku (2008) give a complete summary of this research.

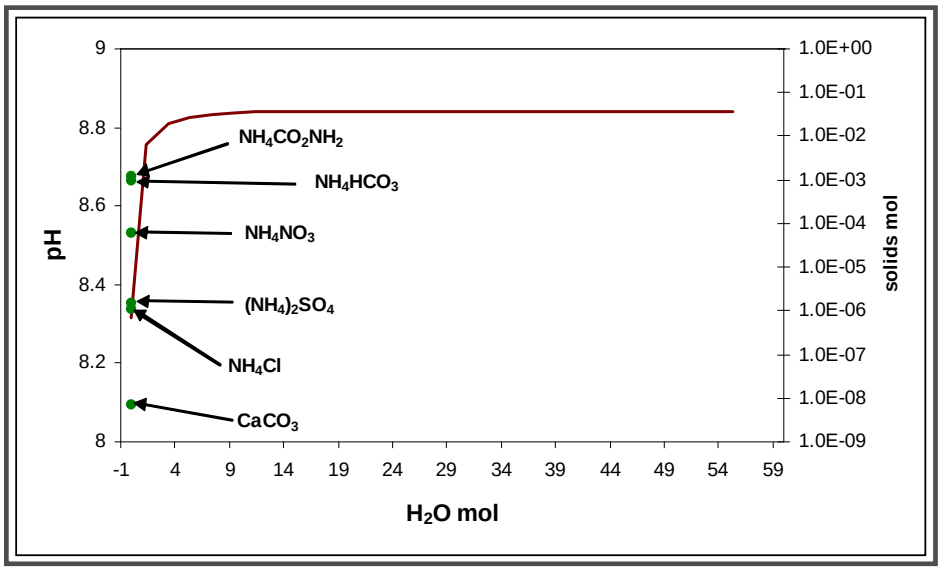

Figure 2. Thermodynamic calculations of the pH and solids formation during drying of AZ-301 condensate samples (1999 sampling).

Phase 3: Experimental Studies

Experimental studies of supernatant drying and CO_2 equilibration was initiated in phase three of this research program. These studies were initiated in FY09 and continued in FY10.

FY09 studies

During FY09 experimental studies were initiated to test/verify the thermodynamic models and provide further insight into the changing supernatant compositions during drying. A total of six different waste tank simulants were prepared for study. This initial effort was complicated by the fact that the reported waste tank analysis in the Best Basis Inventory (BBI) were often not in charge balance. In such cases, the simulants were prepared by using the anion analysis and adding the appropriate concentration of sodium salts to maintain charge balance. This resulted in a final sodium concentration that in some cases was different from the reported values by as much as 20%. The supernatant analysis was also reported to be for the soluble liquid fraction. However, in several cases the total amounts of added components, principally Al, Na, and PO_4, did not dissolve into solution. On an overall basis the thermodynamic models gave a satisfactory prediction of the equilibria in the tank supernatants including the observed oversaturation with respect to aluminum.

After simulant preparation, samples of two simulants (AY-101 and AY-102) were subjected to long-term evaporation in contact with atmospheric CO_2 and the solutions and precipitates were analyzed during the course of the study. The results showed that the solutions (especially, AY-101 which was the most basic) never reached equilibrium with atmospheric CO_2 since the solution water loss was faster than the CO_2 exchange from the

atmosphere. This rapid loss of water relative to the uptake of CO_2 means that the final pH of the evaporating solution will depend upon the relative humidity in the waste tank. If the water content of the headspace gas is very low, the supernatants will evaporate without equilibrating with the atmospheric gases. This can result in the evaporating solutions remaining at pH values more typical of the initial supernatants. However, if the water loss is slowed, for example by increasing the relative humidity during the course of the evaporation, it becomes increasing more likely that the slowly evaporating solutions will come into equilibrium with the tank headspace gases. In such a case the thermodynamic models predict much lower pH values for the evaporating solutions. Felmy and Qafoku (2009) give a complete summary of this research.

FY10 Studies

During FY10, a total of six waste tank simulants covering a broad range of hydroxide, aluminum, and chloride concentrations as well as nitrate/nitrite ratios were prepared and subjected to long-term evaporation in contact with CO_2. The simulant solutions were prepared differently than in FY09 in an attempt to enhance equilibration of the drying supernatant with $CO_2(g)$ and gain additional experimental data to compare with the thermodynamic models. In this procedure the salts were added component by component with reaction time allowed in between. This enabled both a better identification of the specific precipitation reactions that occurred and a more comprehensive data set for comparison with the chemical model. Second, the total inorganic carbon and the bicarbonate/carbonate ratio were adjusted at the start to be as close as possible to the final predicted equilibrium values with respect to CO_2 gas. This step was necessary since our previous studies showed that the large transfers of inorganic carbon from the gas phase to the solution phase could not be achieved without completely evaporating the solutions. Adding the expected amounts of initial inorganic carbon to the solution phase was an attempt to accelerate this exchange equilibrium. The exact procedures are detailed below.

Simulant Preparation

As noted above, the simulant solutions were prepared in a stepwise fashion by addition of salts. The most basic of the salts to be added were sodium carbonate and sodium aluminate. These two salts were added first followed by sodium bicarbonate and then sodium nitrate, sodium nitrite and the other minor components. Adding sodium carbonate and sodium aluminate first resulted in the highest possible initial solution pH and the least possible precipitation of Al containing compounds. Sodium carbonate was initially dissolved in DI-water and the pH was measured immediately upon dissolution. After the addition of sodium aluminate the solutions were stirred for 24 h followed by measuring pH and sampling of the solids that formed. The sodium bicarbonate addition was done in a similar way, the solutions were stirred for 24h, pH measured and solids sampled.

The concentrations of sodium bicarbonate and sodium carbonate to add were determined by first modeling the supernatant composition with the partial pressure of CO_2 fixed at the final equilibrium value. If no solids were predicted to form then the predicted sodium carbonate and sodium bicarbonate concentrations by the model were used to prepare the simulant. However, if solid phases were predicted to form at the equilibration CO_2 concentration, then the starting concentrations of sodium bicarbonate and sodium carbonate had to be adjusted to allow for such reactions to take place while still maintaining the analytical total inorganic carbon concentration required for the simulant. As an example, in the case of the AY101 (segment 3) simulant the CO_2 equilibrated solution had a predicted sodium carbonate concentration of 0.45M and a sodium bicarbonate concentration of 0.09M. However, the model also predicted that 0.09 moles of dawsonite would precipitate from one liter of solution. Therefore, the initial added concentrations of sodium carbonate and sodium bicarbonate had to be adjusted to allow this reaction to occur and still maintain the initial total analytical inorganic carbon concentration (0.63M). Using sodium carbonate and sodium bicarbonate as components, the dawsonite formation reaction can be written as,

$$2NaHCO_3 + NaAlO_2 \rightarrow NaAlCO_3(OH)_2 \text{ (dawsonite)} + Na_2CO_3.$$

The precipitation of dawsonite thus results in the formation of 0.09 moles of sodium carbonate and the consumption of 0.18 moles of sodium bicarbonate. Hence, to allow this reaction to occur and still end up at the final predicted sodium carbonate and sodium bicarbonate concentration, the initial sodium carbonate had to be adjusted to 0.36M (0.45M minus 0.09 moles that will be produced) and the sodium bicarbonate to 0.27M (0.09M plus 0.18 moles that will be consumed) will still maintaining the required total inorganic carbon (0.63M). The initial concentrations of sodium bicarbonate and sodium carbonate for all of the simulants were adjusted in a similar manner. The only exceptions were in cases where the amount of precipitate that was predicted to form was so large that the added sodium carbonate or sodium bicarbonate would not dissolve. In these cases adjustment of the added sodium bicarbonate or sodium carbonate were limited to the expected solubility of the component salts.

Following simulant preparation, the solutions were bubbled for 5 days with a CO_2/air gas mixture with a CO_2 content of 390ppm. The value of 390ppm was taken from an earlier report (Felmy and Qafoku 2008) based upon a literature review of the gas phase compositions found in the DST's. The value of 390ppm was one of the highest and most common values for carbon dioxide found in the DST's. Hence it represents a potential worst case condition with respect to lower pH values of solutions in the DST's. Approximately 200mL of suspension was transferred into a plastic bottle and was purged and dried using 390ppm CO_2 – air mixture. Several times during the evaporation procedure a subsample was collected. At this time the % evaporation for every suspension was calculated. The pH of each subsample was measured and the filtered supernatant was analyzed to determine chemical composition. Sample collection was conducted by first centrifuging a subsample of the suspension at 4000rpm. The supernatant was collected, filtered and analyzed for cations and anions. Anion analysis was conducted using Dionex Ion Chromatography. The other ions Na, K, Al, P, and S were measured with ICP-OES. Inorganic Carbon was measured using persulfate. The solids collected during solution preparations were rinsed with 2mL ethanol, dried at 50^{o}C and ground for solid characterization using X-ray diffractometer Philips X'Pert MPD .

Results and Discussion

In this section the experimental and modeling results for the initial solution preparation and equilibration steps along with the final evaporations will be described. An overall summary of the most significant results will be presented at the end of this section along with a discussion of the possible impact of differences between the measured pH values and the analytically determined hydrogen ion concentration.

Stepwise Preparation of Simulants

A comparison between the observed and predicted pH values as well as the observed and predicted solid phase precipitates that formed during the simulant preparation steps is presented in Figure 3 for all six tank simulants. Overall the model provides good predictions of the solution pH values resulting from the addition of the amount of salt and of the solid phases that should form as the salts are added to the solutions.

The only significant difference between model and experiment occurs after addition of sodium bicarbonate to the AN102 simulant. The model predicts a higher pH value of 12.99 whereas the measured value in solution is only 12.22. Upon addition of sodium bicarbonate the AN102 simulant had the highest initial Al concentration (0.493M). The model predicted that this high initial Al concentration should precipitate (as either dawsonite or $Al(OH)_3$ which would liberate hydroxide and raise the pH, i.e…

$$Al(OH)_4^- = Al(OH)_3\ (c) + OH^-$$

Apparently this reaction did not proceed as far to the right as the model predicts, so less hydroxide is formed and the actual pH is lower than the model prediction.

The thermodynamic modeling predicts $Al(OH)_3$ should form in all simulants after the addition of sodium aluminate. $Al(OH)_3$ could occur in different forms including gibbsite and bayerite. These two phases have the same monoclinic structure and similar solubilities. The XRD analysis shows that the specific $Al(OH)_3$ phase is bayerite. The thermodynamic model also predicts that dawsonite should form in several simulants after the addition of sodium bicarbonate. Evidence for a dawsonite like phase is also found in the XRD analysis (see Figure 4) in terms of the characteristic XRD peak for dawsonite at around 16° 2θ. However, this peak is quite broad and not well defined. Hence we have labeled this phase as "amorphous dawsonite" in Figure 4. Certain XRD patterns also showed evidence for anhydrous sodium carbonate formation even in cases where sodium carbonate was well below saturation. These results have been attributed to the formation of sodium carbonate during the drying of the samples for XRD analysis.

AY101 segment 3 additions	Model		Experimental		Model		Experimental		Model		Experimental	
	pH prediction	solid prediction	pH observation	solid observation	pH prediction	solid prediction	pH observation	solid observation	pH prediction	solid prediction	pH observation	solid observation
Na_2CO_3	11.58	none	11.68	none								
Na_2CO_3+$NaAlO_2$					12.87	$Al(OH)_3$	12.69	Bayerite				
Na_2CO_3+$NaAlO_2$+$NaHCO_3$									10.28	Dawsonite	10.31	amorphous Dawsonite, Bayerite, Na2CO3 as drying product

AY101 segment 8 additions	Model		Experimental		Model		Experimental		Model		Experimental	
	pH prediction	solid prediction	pH observation	solid observation	pH prediction	solid prediction	pH observation	solid observation	pH prediction	solid prediction	pH observation	solid observation
Na_2CO_3	11.76	none	11.97	none								
Na_2CO_3+$NaAlO_2$					13.53	$Al(OH)_3$	13.2	Bayerite				
Na_2CO_3+$NaAlO_2$+$NaHCO_3$									12.95	$Al(OH)_3$	12.8	Bayerite

AY102 additions	Model		Experimental		Model		Experimental		Model		Experimental	
	pH prediction	solid prediction	pH observation	solid observation	pH prediction	solid prediction	pH observation	solid observation	pH prediction	solid prediction	pH observation	solid observation
Na_2CO_3	11.58	none	11.68	none								
Na_2CO_3+$NaAlO_2$					12.23	$Al(OH)_3$	11.74	none				
Na_2CO_3+$NaAlO_2$+$NaHCO_3$									10.21	Dawsonite	10.32	amorphous Dawsonite, Bayerite, small Trona, Na2CO3 as drying

Figure 3. Comparison of experimentally determined pH values and precipitates with modeling simulations, upon the addition of specific salts. For each tank simulant the first row shows the results for addition of Na_2CO_3 only. The second row Na_2CO_3 plus $NaAlO_2$ and the third row addition of $NaHCO_3$ to the Na_2CO_3 plus $NaAlO_2$ mixture.

Figure 3. Continued

AN102 additions	Model		Experimental		Model		Experimental		Model		Experimental	
	pH prediction	solid prediction	pH observation	solid observation	pH prediction	solid prediction	pH observation	solid observation	pH prediction	solid prediction	pH observation	solid observation
Na_2CO_3	11.84	none	12.04	none								
Na_2CO_3+$NaAlO_2$					13.75	$Al(OH)_3$	13.45	Bayerite				
Na_2CO_3+$NaAlO_2$+$NaHCO_3$									12.99	Dawsonite, $Al(OH)_3$	12.22	amorphous Dawsonite, Bayerite, Na2CO3 as drying product

SY102 high Cl additions	Model		Experimental		Model		Experimental		Model		Experimental	
	pH prediction	solid prediction	pH observation	solid observation	pH prediction	solid prediction	pH observation	solid observation	pH prediction	solid prediction	pH observation	solid observation
Na_2CO_3	11.73	none	11.84	none								
Na_2CO_3+$NaAlO_2$					13.83	$Al(OH)_3$	13.51	Bayerite				
Na_2CO_3+$NaAlO_2$+$NaHCO_3$									13.65	$Al(OH)_3$	13.59	Bayerite

SY102 high NO_3 additions	Model		Experimental		Model		Experimental		Model		Experimental	
	pH prediction	solid prediction	pH observation	solid observation	pH prediction	solid prediction	pH observation	solid observation	pH prediction	solid prediction	pH observation	solid observation
Na_2CO_3	11.48	none	11.67	none								
Na_2CO_3+$NaAlO_2$					12.73	$Al(OH)_3$	12.56	Bayerite				
Na_2CO_3+$NaAlO_2$+$NaHCO_3$									10.33	Dawsonite	10.31	amorphous Dawsonite, Bayerite, Na2CO3 as drying product

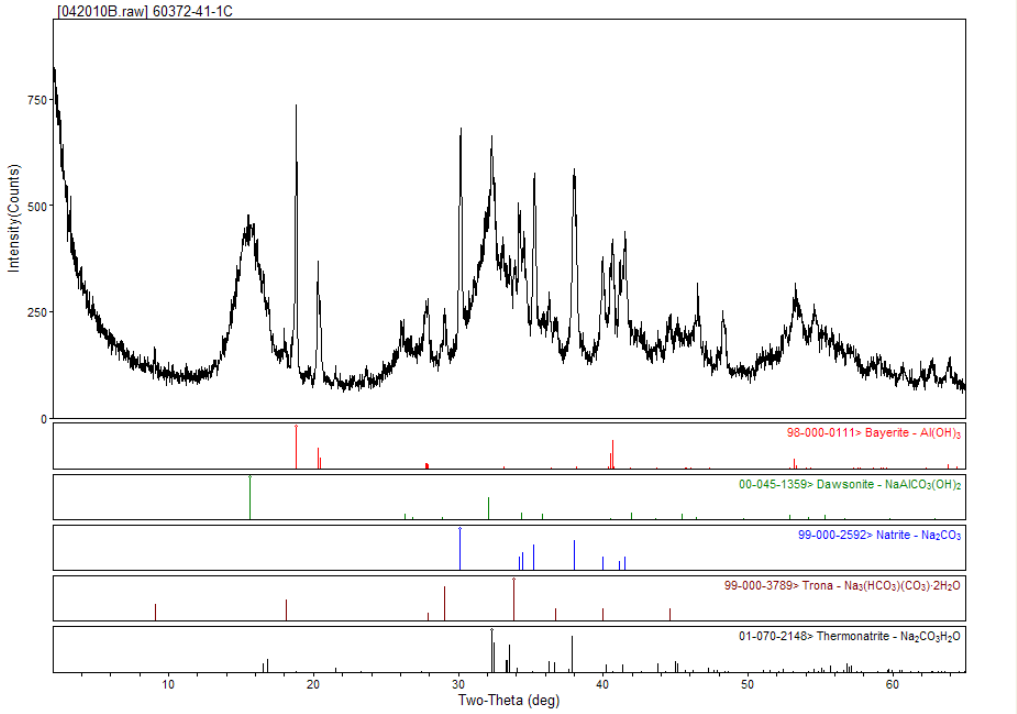

Figure 4. XRD pattern for tank AY101 (segment 3) simulant after the addition of Na_2CO_3, $NaAlO_2$, and $NaHCO_3$.

Simulant Evaporation and CO_2 Equilibration.

Following simulant preparation the solutions were bubbled with CO_2 at a concentration of 390ppm for as long as 42 days. The simulants were sampled at different times during this CO_2 equilibration/evaporation process and the pH, solution phase concentrations and solid phase precipitates were determined. The simulants were first sampled after 5 days of bubbling with CO_2 to allow time for equilibration of the starting solutions with CO_2 without undergoing significant evaporation. The water content of the solutions at this point was then used as a reference for subsequent water removal ratios by weighing the solutions at each sample point. Knowledge of the water content was necessary to allow exact comparisons between model and experiment. The results are presented below for each individual simulant.

Tank AY-101 (segment 3) Simulant

The tank AY-101 segment 3 simulant was one of the lowest concentration stimulants studied with a total Na concentration of 2.3M. The dominant anions are nitrate and carbonate. The model predictions of pH and electrolyte concentrations (Table 1a) compare very well with the analytical data even to high evaporation. The model predicts the major precipitate to be dawsonite all the way through the evaporation sequence. There is some evidence for formation of a small amount of dawsonite in the initial sample (0% evaporation, Figure 5). However, the XRD analysis suggests that bayerite is more prevalent. The model also predicts that trona should form in the final evaporation step. The XRD pattern also shows a minor characteristic peak for trona in the final evaporation (76%). However, this is a minor phase. The XRD pattern is dominated by $NaNO_3$ which apparently forms during evaporation of the sample for XRD.

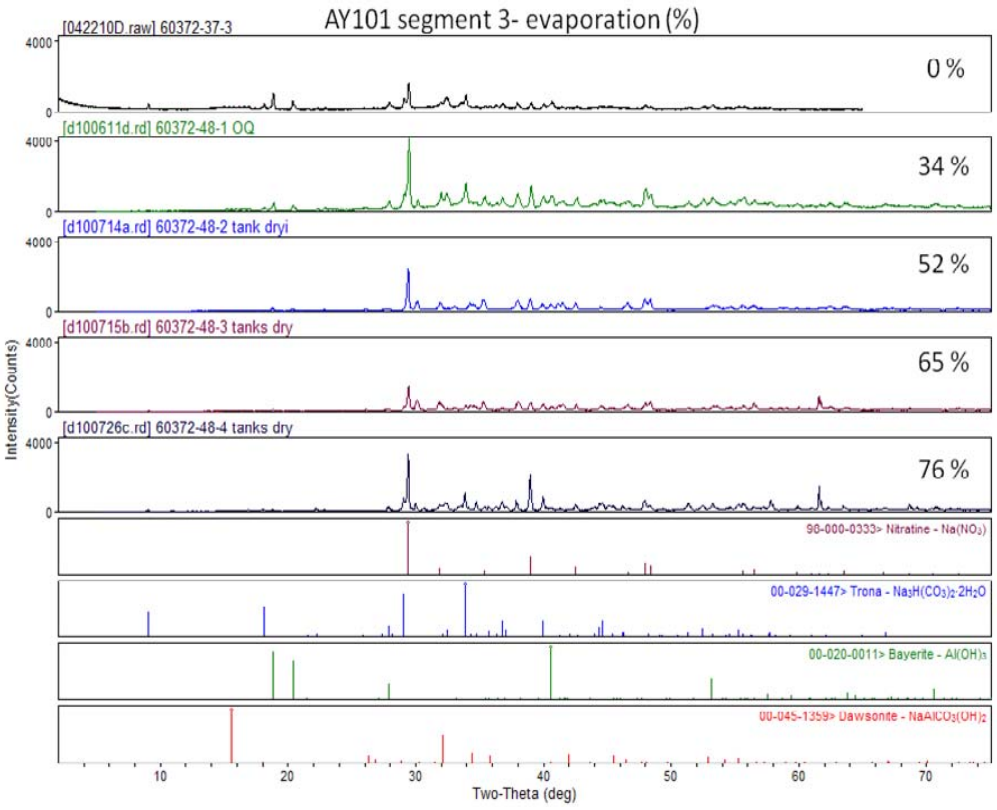

Figure 5. XRD patterns fro samples collected during the evaporation of Tank AY-101 (segment 3) simulant.

In summary, for the AY-101 segment 3 simulant the model gives a very good prediction of the overall chemistry of the solution even to high evaporation. The major disagreement is that the model predicts formation of dawsonite whereas bayerite appears to actually form. Formation of bayerite rather than dawsonite does not significantly impact the predicted Al concentration since both solids maintain low Al concentrations at these pH values.

Tank AY-101 (segment 8) Simulant

The tank AY-101 segment 8 simulant contained significantly higher total Na concentration than the segment 3 simulant, 4.95M versus 2.3M. The major anions are nitrate, carbonate and nitrite. In contrast to the excellent prediction of pH and electrolyte concentration for the segment 3 simulant, the predictions of pH and inorganic carbon concentration for the segment 8 simulant are uniformly lower than the experimental observations (Table 1b). In all cases the model predicts lower concentrations of inorganic carbon and lower pH values than observed. The model predicts dawsonite should form throughout the evaporation sequence with trona formation occurring by the 49% evaporation point. The XRD analysis does not support the formation of either dawsonite or trona. Instead the XRD analysis shows the formation of bayerite throughout the evaporation sequence and thermonatrite in the final step (Figure 4). This discrepancy in solid phase formation appears to be the explanation for the differences between model and experiment. In order to reach equilibrium large quantities of dawsonite must form (~0.35 moles). However, during this study dawsonite does not form. Instead bayerite precipitates which liberates large quantities of hydroxide from the added aluminate i.e.

$$Al(OH)_4^- = Al(OH)_3 + OH^-$$

therefore a high pH is observed. Since dawsonite does not form the measured inorganic carbon is also higher than the model prediction.

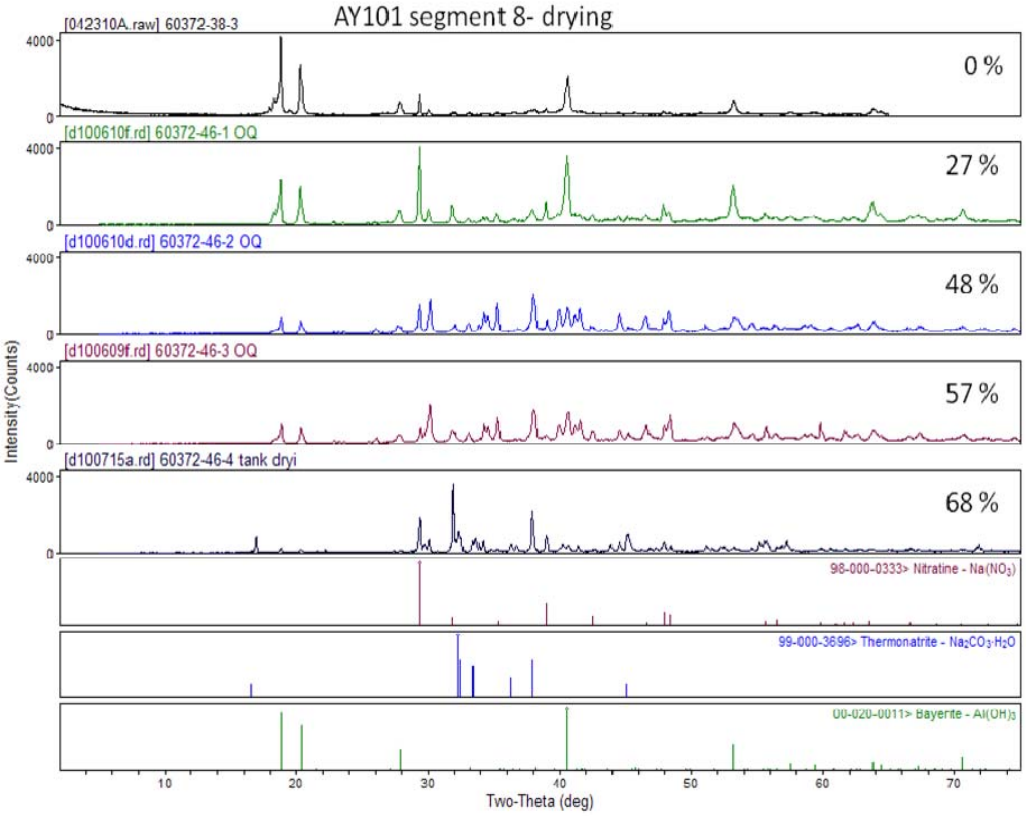

Figure 6. XRD patterns for samples collected during the evaporation of tank AY-101 (segment 8) simulant.

Table 1. Experimental and predicted electrolyte concentrations and pH values for tank AY-101 simulants (a) segment 3, (b) segment 8, as a function of solution evaporation.

(a)

5 Day Sampling (0% Evaporation)

	Experiment	Predicted
Na	2.284	2.30
K	<0.0038	
Al	<0.0003	$8.4x10^{-8}$
Br	<0.0125	0.0048
Cl	<0.0141	0.013
Cr	0.002	$8.7x10^{-7}$
F	<0.0105	0.0105
NO_3	0.963	1.01
NO_2	0.158	0.167
P	0.042	0.04
S	0.017	0.0153
Inorganic C	0.572	0.536
pH	10.220	10.15

17 Day Sampling (34.37% Evaporation)

	Experiment	Predicted
Na	3.654	3.41
K	0.000	
Al	0.000	$5.4x10^{-8}$
Br	<0.1252	0.0071
Cl	0.000	0.02
Cr	0.003	$4.26x10^{-7}$
F	<0.1053	0.0156
NO_3	0.000	1.49
NO_2	0.000	0.248
P	0.069	0.06
S	0.027	0.023
Inorganic C	0.839	0.782
pH	10.160	10.23

25 Day Sampling (52.04% Evaporation)

	Experiment	Predicted
Na	4.78	4.53
K	0.00	
Al	0.00	$3.8x10^{-8}$
Br	<0.1252	0.0094
Cl	0.00	0.026
Cr	0.00	$2.6x10^{-7}$
F	<0.1053	0.021
NO_3	0.00	1.98
NO_2	0.00	0.33
P	0.09	0.079
S	0.03	0.03
Inorganic C	1.17	1.03
pH	10.12	10.31

34 Day Sampling (64.87% Evaporation)

	Experiment	Predicted
Na	6.220	5.93
K	0.002	
Al	0.000	$2.6x10^{-8}$
Br	<0.1252	0.0123
Cl	0.000	0.035
Cr	0.006	$1.67x10^{-7}$
F	<0.1053	0.027
NO_3	0.000	2.6
NO_2	0.000	0.43
P	0.119	0.104
S	0.045	0.039
Inorganic C	1.414	1.35
pH	10.290	10.42

42 Day Sampling (76.03% Evaporation)

	Experiment	Predicted
Na	8.090	6.85
K	0.003	
Al	0.000	$1.9x10^{-8}$
Br	<0.1252	0.017
Cl	0.000	0.048
Cr	0.009	$1.2x10^{-7}$
F	<0.1053	0.038
NO_3	0.000	3.59
NO_2	0.000	0.6
P	0.097	0.144
S	0.067	0.055
Inorganic C	1.383	1.15
pH	11	10.43

(b)

5 Day Sampling (0% Evaporation)

	Experiment	Predicted
Na	4.959	4.48
K	0.044	0.04
Al	0.021	$3.5x10^{-8}$
Br	<0.0125	
Cl	0.096	0.086
Cr	0.004	$2.7x10^{-7}$
F	<0.0105	0.0099
NO_3	1.589	1.58
NO_2	0.909	0.972
P	0.049	0.043
S	0.038	0.033
Inorganic C	1.124	0.92
pH	12.51	10.29

14 Day Sampling (27.36% Evaporation)

	Experiment	Predicted
Na	6.612	5.90
K	0.064	0.053
Al	0.011	$2.3x10^{-8}$
Br	<0.1252	
Cl	0.160	0.11
Cr	0.006	$1.8x10^{-7}$
F	<0.1053	0.013
NO_3	2.048	2.08
NO_2	1.346	1.28
P	0.067	0.057
S	0.056	0.044
Inorganic C	1.397	1.21
pH	11.420	10.39

24 Day Sampling (48.49% Evaporation)

	Experiment	Predicted
Na	8.35	6.77
K	0.10	0.071
Al	0.00	$1.7x10^{-8}$
Br	<0.1252	
Cl	0.19	0.15
Cr	0.01	$1.4x10^{-7}$
F	<0.1053	0.017
NO_3	2.95	2.79
NO_2	2.00	1.72
P	0.07	0.076
S	0.08	0.059
Inorganic C	1.50	1.02
pH	11.22	10.39

32 Day Sampling (57.36% Evaporation)

	Experiment	Predicted
Na	9.482	7.16
K	0.121	0.082
Al	0.002	$1.3x10^{-8}$
Br	<0.1252	
Cl	0.226	0.18
Cr	0.010	$1.3x10^{-7}$
F	<0.1053	0.02
NO_3	3.629	3.22
NO_2	2.500	1.98
P	0.074	0.088
S	0.104	0.068
Inorganic C	1.339	0.825
pH	11.290	10.37

37 Day Sampling (67.95% Evaporation)

	Experiment	Predicted
Na	9.656	8.17
K	0.171	0.105
Al	0.002	$1.1x10^{-8}$
Br	<0.1252	
Cl	0.299	0.23
Cr	0.014	$1.1x10^{-7}$
F	<0.1053	0.026
NO_3	3.403	4.15
NO_2	3.847	2.55
P	0.065	0.11
S	0.125	0.087
Inorganic C	1.036	0.508
pH	11.68	10.32

Tank AY-102 Simulant

The tank AY-102 simulant was the most dilute solution examined, Na concentration 1.2M. The major anions were carbonate and nitrite. Overall, the model predictions of the pH changes and electrolyte concentration were very satisfactory (Table 2). No major discrepancies were observed. The model predicts that dawsonite should form throughout the evaporation sequence with trona formation only in the last evaporation step. There is evidence for some dawsonite formation in the XRD pattern of the precipitated solids initially (0% evaporation in Figure 7). However, the predicted amount of dawsonite is small (0.02 moles) and most of the solids that are determined by XRD are comprised of Na_2CO_3 that apparently forms during the drying of solutions for XRD analysis. However in the final evaporation step there is clear evidence for trona formation, exactly as predicted by the model.

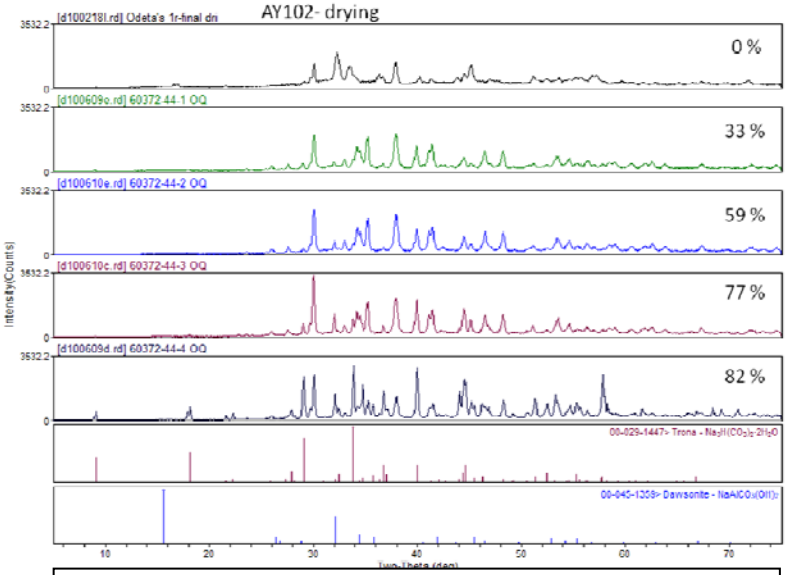

Figure 7. XRD patterns for samples collected during the evaporation of tank AY-102 simulant.

Tank AN-102 Simulant

The tank AN-102 simulant was one of the prepared simulant with the highest salt concentration and the highest initial Al concentrations (0.493 moles). Hence, higher amounts of inorganic carbon had to be added to the initial solutions to account for the large amount of dawsonite that was predicted to form. The model predicted dawsonite and trona formation throughout the evaporation sequence. However, the XRD results show no evidence that either phase formed. The solids are dominated by $NaNO_3$ that formed upon drying along with some bayerite and possibly thermonatrite (Figure 8). Since the equilibrium model prediction (formation of large amounts of dawsonite 0.45 moles) did not occur, the solution pH and the inorganic carbon remained higher than model prediction. This is the same situation as occurred with the tank AY-101 segment 8 simulant.

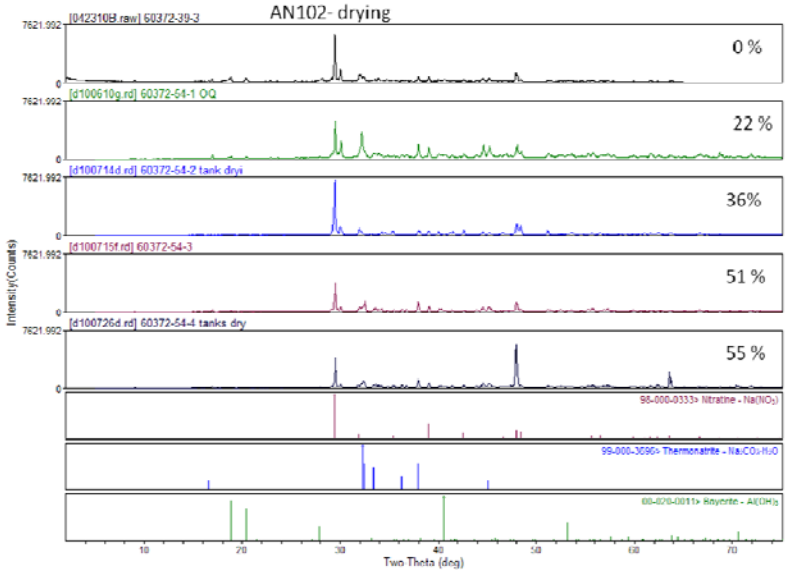

Figure 8. XRD patterns for samples collected during the evaporation of tank AN-102 simulant.

Table 2. Experimental and predicted electrolyte concentrations and pH values for tank AY-102 simulant (a) and tank AN-102 simulant (b) as a function of simulant evaporation.

(a)

5 Day Sampling (0% Evaporation)

	Experiment	Predicted
Na	1.196	1.22
K	0.004	0.004
Al	<0.0003	1.6×10^{-7}
Br	<0.0125	0.015
Cl	<0.0141	0.001
Cr	<0.0001	
F	<0.0105	0.001
NO_3	0.019	0.004
NO_2	0.313	0.293
P	0.011	0.011
S	0.007	0.008
Inorganic C	0.511	0.485
pH	10.24	10.17

14 Day Sampling (32.95% Evaporation)

	Experiment	Predicted
Na	1.827	1.81
K	0.006	0.0059
Al	<0.0001	1.1×10^{-7}
Br	<0.1252	0.022
Cl	<0.1410	0.0015
Cr	0.000	
F	<0.1053	0.0015
NO_3	<0.1613	0.0059
NO_2	0.470	0.434
P	0.017	0.016
S	0.013	0.012
Inorganic C	0.783	0.704
pH	10.210	10.23

24 Day Sampling (58.97% Evaporation)

	Experiment	Predicted
Na	2.93	2.91
K	0.01	0.0094
Al	<0.0001	6.8×10^{-8}
Br	<0.1252	0.035
Cl	<0.1410	0.0024
Cr	0.00	
F	<0.1053	0.0024
NO_3	<0.1613	0.0094
NO_2	0.72	0.697
P	0.03	0.026
S	0.02	0.019
Inorganic C	1.24	1.11
pH	10.07	10.31

32 Day Sampling (77.06% Evaporation)

	Experiment	Predicted
Na	5.263	5.02
K	0.019	0.016
Al	<0.0001	3.6×10^{-8}
Br	<0.1252	0.061
Cl	<0.1410	0.0041
Cr	0.000	
F	<0.1053	0.0041
NO_3	<0.1613	0.016
NO_2	1.426	1.2
P	0.052	0.045
S	0.038	0.032
Inorganic C	2.045	1.89
pH	10.160	10.44

35 Day Sampling (82.14% Evaporation)

	Experiment	Predicted
Na	6.133	5.79
K	0.028	0.02
Al	0.000	2.9×10^{-8}
Br	0.126	0.077
Cl	<0.1410	0.0051
Cr	0.000	
F	<0.1053	0.0051
NO_3	<0.1613	0.02
NO_2	1.958	1.51
P	0.073	0.056
S	0.052	0.041
Inorganic C	1.992	2.11
pH	10.71	10.48

(b)

5 Day Sampling (0% Evaporation)

	Experiment	Predicted
Na	8.699	6.59
K	0.043	0.033
Al	<0.0003	1.9×10^{-8}
Br	<0.0125	0.0066
Cl	0.094	0.078
Cr	0.005	1.5×10^{-7}
F	<0.0105	0.0025
NO_3	3.064	2.55
NO_2	1.432	1.52
P	0.067	0.05
S	0.156	0.11
Inorganic C	1.565	1.15
pH	11.07	10.41

17 Day Sampling (22.49% Evaporation)

	Experiment	Predicted
Na	9.091	7.11
K	0.057	0.041
Al	0.000	1.6×10^{-8}
Br	<0.1252	0.0081
Cl	0.000	0.097
Cr	0.006	1.3×10^{-7}
F	<0.1053	0.0031
NO_3	0.000	3.17
NO_2	0.000	1.89
P	0.077	0.062
S	0.173	0.14
Inorganic C	1.301	0.861
pH	11.290	10.38

25 Day Sampling (36.35% Evaporation)

	Experiment	Predicted
Na	9.66	7.66
K	0.07	0.048
Al	0.00	1.3×10^{-8}
Br	<0.1252	0.0095
Cl	0.00	0.11
Cr	0.01	1.2×10^{-7}
F	<0.1053	0.0036
NO_3	0.00	3.71
NO_2	0.00	2.21
P	0.07	0.073
S	0.15	0.16
Inorganic C	1.21	0.655
pH	11.53	10.35

34 Day Sampling (50.99% Evaporation)

	Experiment	Predicted
Na	9.830	8.62
K	0.088	0.058
Al	0.000	9.7×10^{-9}
Br	<0.1252	0.012
Cl	0.000	0.14
Cr	0.009	1.1×10^{-7}
F	<0.1053	0.0044
NO_3	0.000	4.51
NO_2	0.000	2.69
P	0.063	0.089
S	0.114	0.2
Inorganic C	1.013	0.424
pH	11.660	10.31

35 Day Sampling (54.68% Evaporation)

	Experiment	Predicted
Na	9.613	8.93
K	0.084	0.061
Al	0.000	8.8×10^{-9}
Br	<0.1252	0.012
Cl	0.000	0.15
Cr	0.008	1.1×10^{-7}
F	<0.1053	0.0046
NO_3	0.000	4.76
NO_2	0.000	2.84
P	0.069	0.094
S	0.087	0.19
Inorganic C	1.005	0.37
pH	11.46	10.3

Tank SY-102 (High Nitrate) Simulant

The tank SY-102 simulant with high nitrate concentration (~4M) had the highest nitrate concentration of any of the stimulants studied. The initial Al concentration was also relatively low (0.069M). In general the model predictions of the pH changes and electrolyte concentrations were very good. The model predicted that dawsonite should form throughout the evaporation sequence with trona and $NaNO_3$ precipitating in the next to the last evaporation step (i.e. 60% evaporation). The XRD analysis is completely dominated by the peaks for $NaNO_3$ (Figure 9). There is no evidence for trona formation. The analysis of the supernatants supports this lack of trona formation since the inorganic carbon concentration increases from the 34 to the 42 day sampling (Table 3a). The absence of trona formation in the last evaporation step is the only significant difference between model and experiment.

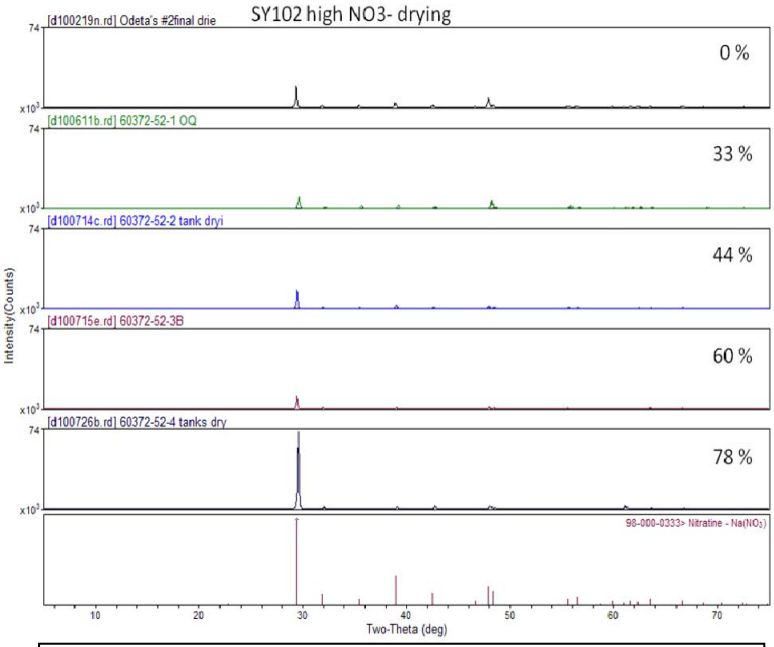

Figure 9. XRD patterns for samples collected during the evaporation of tank SY-102 (high nitrate) simulant.

Tank SY-102 (High Chloride) Simulant

The final tank simulant examined was a tank SY-102 simulant with high chloride concentration (0.16M). The predominant anions are nitrate, carbonate, and nitrite. The initial Al concentration was very high (0.65M). Hence, the model predicted that large quantities of dawsonite should form upon equilibration of the solutions with CO_2(g) (i. e. 0.65 moles). Precipitation of such large quantities of dawsonite does not occur as the principal Al containing precipitate is bayerite (see Figure 10). Hence the solution pH values and total inorganic carbon concentrations are higher than the model predictions (Table 3b). This is the exact same chemistry that was observed for tank simulants AN-102 and AY-101 segment 8. Interestingly the model predicts the formation of a small amount of the NaF Na_2SO_4 double salt in the late stages of evaporation. Although there is no clear evidence for this in the XRD pattern, the analytical sulfur concentration does decrease from the 34 day to the 42 day sampling period in agreement with the model predictions (Table 3b).

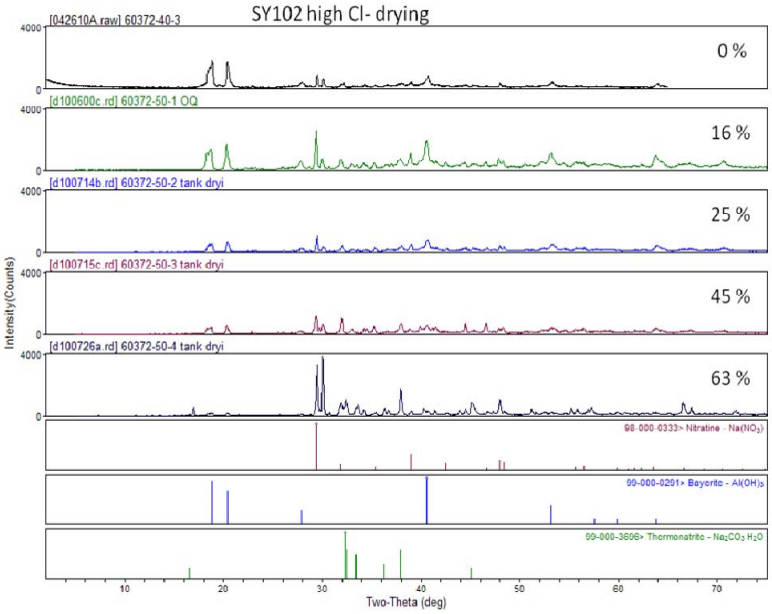

Figure 10. XRD patterns for samples collected during the evaporation of tank SY-102 (high chloride) simulant.

Table 3. Experimental and predicted electrolyte concentrations and pH values for tank SY102 simulants at both high nitrate concentration (a) and high Cl concentration (b) as a function of simulant evaporation.

(a)

5 Day Sampling (0% Evaporation)		
	Experiment	Predicted
Na	4.959	4.49
K	<0.0038	0.00086
Al	<0.0003	3.5×10^{-8}
Br	<0.0125	0.064
Cl	<0.0141	0.011
Cr	0.011	1.8×10^{-7}
F	<0.0105	0.0026
NO_3	4.145	3.64
NO_2	0.111	0.097
P	0.028	0.024
S	0.057	0.047
Inorganic C	0.366	0.295
pH	9.9	10.01

17 Day Sampling (32.81% Evaporation)		
	Experiment	Predicted
Na	6.916	6.19
K	0.004	0.0012
Al	0.000	2.1×10^{-8}
Br	<0.1252	0.088
Cl	0.000	0.015
Cr	0.015	9.4×10^{-8}
F	<0.1053	0.0036
NO_3	0.000	5.02
NO_2	0.000	0.13
P	0.036	0.033
S	0.075	0.064
Inorganic C	0.479	0.405
pH	9.960	10.16

25 Day Sampling (43.82% Evaporation)		
	Experiment	Predicted
Na	7.66	7.09
K	0.01	0.0014
Al	0.00	1.6×10^{-8}
Br	<0.1252	0.1
Cl	0.00	0.018
Cr	0.02	7.5×10^{-8}
F	<0.1053	0.0041
NO_3	0.00	5.75
NO_2	0.00	0.15
P	0.04	0.038
S	0.08	0.074
Inorganic C	0.53	0.464
pH	10.00	10.24

34 Day Sampling (60.42% Evaporation)		
	Experiment	Predicted
Na	7.960	8.36
K	0.006	0.0018
Al	0.000	1.1×10^{-8}
Br	<0.1252	0.13
Cl	0.000	0.023
Cr	0.024	6.2×10^{-8}
F	<0.1053	0.0054
NO_3	0.000	6.76
NO_2	0.000	0.2
P	0.059	0.05
S	0.122	0.097
Inorganic C	0.752	0.517
pH	10.040	10.36

42 Day Sampling (77.53% Evaporation)		
	Experiment	Predicted
Na	8.308	8.56
K	0.008	0.0032
Al	0.000	1.1×10^{-8}
Br	<0.1252	0.23
Cl	0.000	0.041
Cr	0.045	6.8×10^{-8}
F	<0.1053	0.0095
NO_3	0.000	6.52
NO_2	0.000	0.35
P	0.096	0.088
S	0.201	0.17
Inorganic C	1.127	0.495
pH	10.19	10.35

(b)

5 Day Sampling (0% Evaporation)		
	Experiment	Predicted
Na	6.090	5.06
K	0.060	0.052
Al	0.077	2.8×10^{-8}
Br	<0.0125	0.0052
Cl	0.156	0.13
Cr	0.006	2.2×10^{-7}
F	0.090	0.087
NO_3	2.129	1.79
NO_2	1.300	1.43
P	0.021	0.0445
S	0.026	0.022
Inorganic C	1.099	0.82
pH	12.990	10.27

17 Day Sampling (15.69% Evaporation)		
	Experiment	Predicted
Na	7.264	5.84
K	0.076	0.06
Al	0.057	2.3×10^{-8}
Br	<0.1252	0.006
Cl	0.000	0.16
Cr	0.007	1.8×10^{-7}
F	<0.1053	0.1
NO_3	0.000	2.07
NO_2	0.000	1.65
P	0.016	0.051
S	0.030	0.025
Inorganic C	1.251	0.946
pH	13.080	10.33

25 Day Sampling (25.32% Evaporation)		
	Experiment	Predicted
Na	8.09	6.46
K	0.08	0.067
Al	0.05	1.9×10^{-8}
Br	<0.1252	0.0067
Cl	0.00	0.17
Cr	0.01	1.7×10^{-7}
F	<0.1053	0.11
NO_3	0.00	2.28
NO_2	0.00	1.83
P	0.01	0.057
S	0.03	0.028
Inorganic C	1.46	1.05
pH	13.03	10.38

34 Day Sampling (44.51% Evaporation)		
	Experiment	Predicted
Na	9.439	7.26
K	0.125	0.086
Al	0.035	1.5×10^{-8}
Br	<0.1252	0.0086
Cl	0.000	0.22
Cr	0.011	1.4×10^{-7}
F	<0.1053	0.14
NO_3	0.000	2.92
NO_2	0.000	2.34
P	0.008	0.073
S	0.017	0.036
Inorganic C	1.141	0.813
pH	12.770	10.36

42 Day Sampling (62.86% Evaporation)		
	Experiment	Predicted
Na	9.917	8.54
K	0.174	0.12
Al	0.002	9.7×10^{-9}
Br	<0.1252	0.012
Cl	0.000	0.3
Cr	0.016	1.2×10^{-7}
F	<0.1053	0.13
NO_3	0.000	4
NO_2	0.000	3.2
P	0.010	0.1
S	0.013	0.015
Inorganic C	0.837	0.442
pH	11.53	10.29

Impact on Waste Tank Steel Corrosion

The previous discussion describes the changes in chemical composition that occur as the supernatants dry and adsorb atmospheric gases. As part of this overall research program experimental studies were also initiated on the possible impacts of such changes on waste tank steel corrosion. The research on steel corrosion was performed primarily at SRNL (see Hoffman 2010 for a complete description of this research). However, samples of the tank steels following corrosion testing at SRNL were sent to the Environmental Molecular Sciences Laboratory (EMSL) at PNNL to undergo examination by high resolution scanning electron microscopy (SEM) and associated use of a focused ion beam (FIB) to remove surface corrosion layers and identify possible mechanisms of steel corrosion. During FY10, it was possible to examine the principal tank steel sample identified by SRNL as having experienced significant corrosion. This sample had been exposed to the SY102 simulant with high nitrate concentration and relatively low pH (see Table 3a).

The electron micrographs of the corrosion layer, Figure 11, show two different regions of variable Fe and chloride content as well as evidence of Sn and Sb on the surface. The chloride, Sn and Sb result from the treatment of the surface with Clarke's solution to remove the surface oxide layer and expose the metal corrosion.

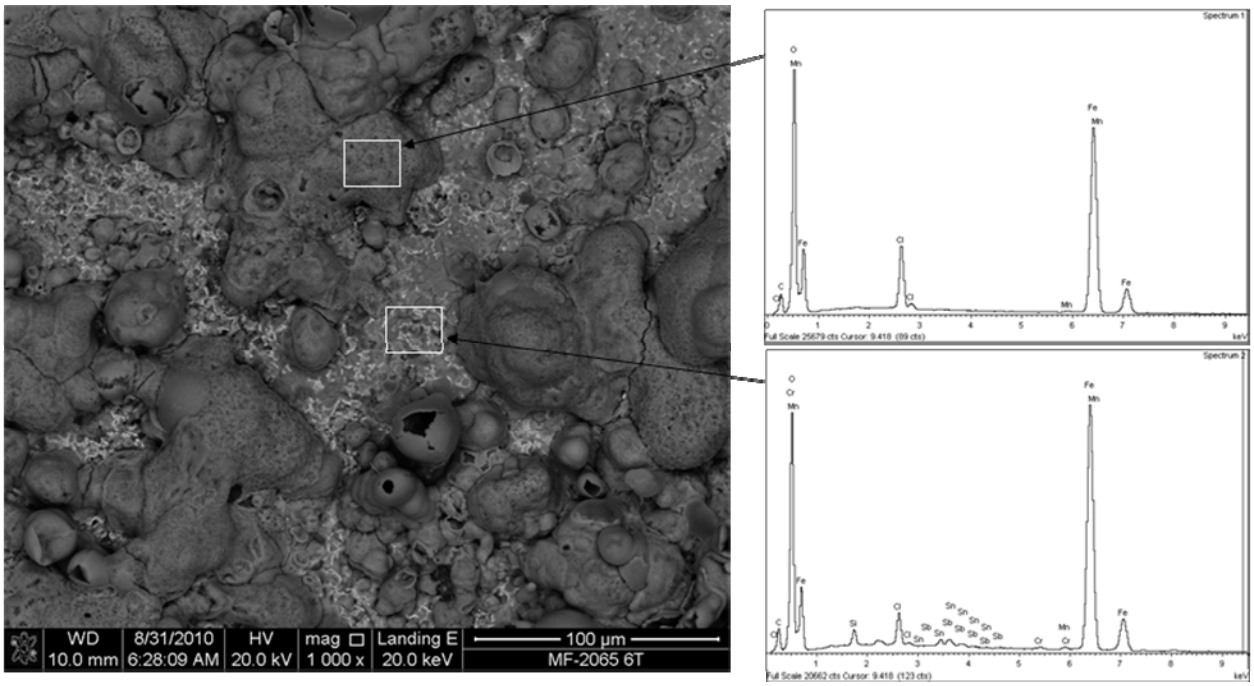

Figure 11. SEM image of tank steel exposed to SY102 high nitrate solution showing region of different surface composition.

The steel sample was then milled with the FIB to examine the effects of corrosion with depth (Figure 12). The results show extensive pitting of the surface to depths of approximately 10µm.

It was also of interest to examine steel samples subjected to exposure to the same SY102 high nitrate solution where the oxide film on the steel surface had not been removed. In this regard we had placed samples of tanks steel in the evaporating SY102 high nitrate solution and these samples had remained in solution for the entire course of the evaporation study. SEM micrographs of these samples show the development of an extensive oxide surface coating over the entire surface. FIB milling of the surface film reveals an oxide surface film of

approximately 20µm in depth as well as evidence of corrosion pitting in the surface (middle left in Figure 13) in agreement with the findings for the samples tested at SRNL.

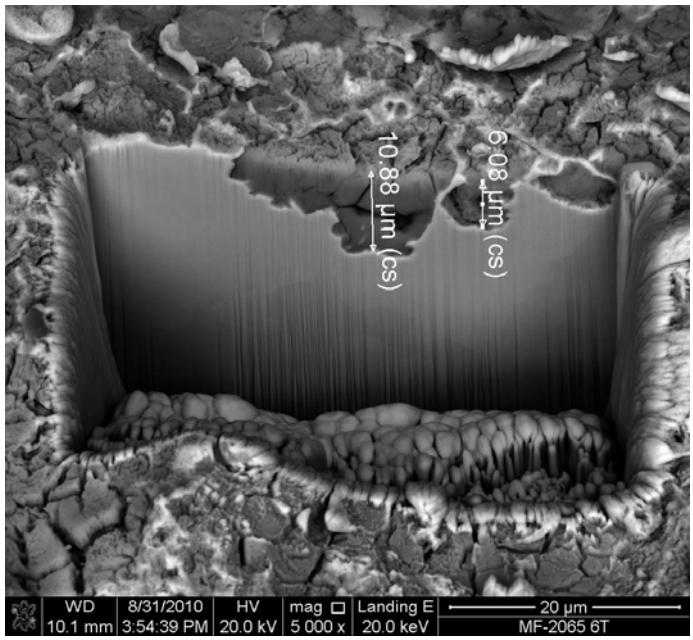

Figure 12. SEM image of tank steel exposed to SY102 high nitrate solution following FIB milling. The cross section shows evidence of corrosion pitting extending to approximately 10µm depth.

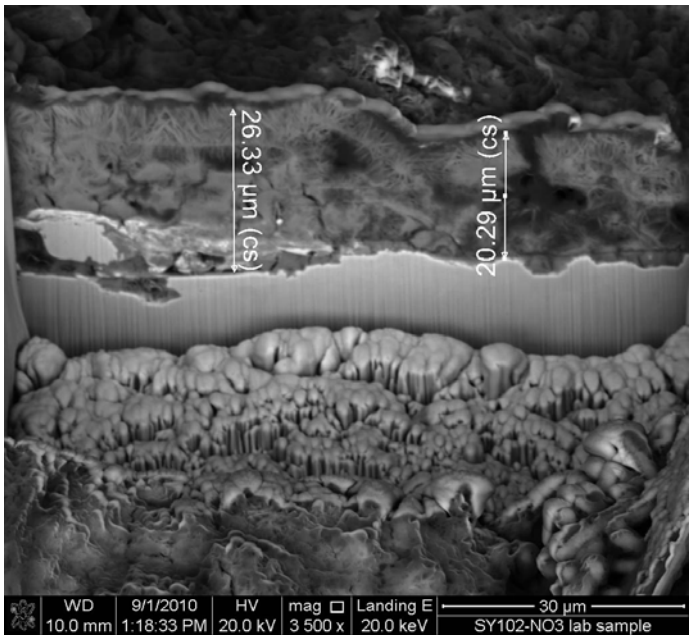

Figure13. SEM images of tank steels subjected to evaporating SY102 high nitrate solutions.

Estimation of pH values

Finally, it is of interest to determine the importance of the predicted and experimental pH values in determining differences in solution chemistry. This issue is especially important for tank solutions which react with atmospheric CO_2 since such reactions can reduce the free hydroxide concentrations to levels which are too low to determine analytically. The pH is defined as the negative logarithm of the activity of hydrogen ion. However, in theory it is not possible to measure a single ion activity since the necessity of maintaining electroneutrality in solution means that only the activity of neutral electrolytes or salts can be measured. Hence all efforts to derive or estimate a single ion activity are based upon certain conventions or approximations. As a result, the current practice of determining the corrosion potential of electrolyte solutions based upon the measured pH has an unknown convention dependence and it is desirable to at least know how such measurements compare to convention independent measurements of solution properties.

Although the single ion activity of a solution cannot theoretically be measured, the hydrogen ion concentration of a solution is a measurable property. In fact a variety of techniques, including use of cells with and without liquid junctions and the use of organic indicator species have been used to determine the hydrogen ion concentration. Unfortunately, several of these methods are difficult to apply to waste tank solutions. For example, the use of organic indicator species requires the knowledge of pKa values for the anonic species as a function of electrolyte concentration and the use of cells without liquid junctions requires a thermodynamic model to calculate electrolyte activity coefficients or activity coefficient ratios (Rai, et al., 1995).

In the case of cells with liquid junctions, for example a glass electrode with a calomel reference, a liquid junction potential (or difference in liquid junction potentials) is introduced and only a combination of single ion activity terms and liquid junction potentials is measured (see Mesmer 1991). This liquid junction term, or a selected combination of liquid junction terms and activity terms, must then be determined either by calculation (such as the use of the Henderson equation) or by selected gran or other titrations with known amounts

of acid or base. The advantage of this method is that in certain solutions where no acid or base consuming species are present the hydrogen ion concentration can be determined directly without resorting to the use of a thermodynamic model.

In this approach, the H^+ concentration (pC_H+) in unknown samples of a given electrolyte of fixed molarity can be estimated using a glass electrode with liquid junction from the following equation (see Rai et al. 1995) for a derivation).

$$pC_H+ = pH_{ob} + A \quad (1)$$

where pH_{ob} is the observed reading with the calibrated combination glass electrode of the unknown sample, and A is defined by

$$A = \log \gamma_H+ + (F/2.303RT)\Delta E_j \quad (2)$$

where γ_H+ is the convention-dependent molarity-scale activity coefficient of H^+, and ΔE_j is the difference in liquid junction potential between standards and solutions. Neither term on the right-hand side of Eq. (2) is individually measurable, but the combination can be measured.

Rewriting Eq. (1) in terms of logarithms, taking the antilog of both sides and rearranging, yields

$$H^+_{ob} = 10^A C_H+ \quad (3)$$

The constant A is then obtained by a modified Gran titration (as describe under experimental procedures) in which the moles of added free acid or base per liter are plotted against H^+_{ob} (i.e., 10^{-pHob}). The logarithm of the slope of this curve is the correction factor A needed to convert the observed pH reading to pC_{H+}.

As part of this study, the A values needed to convert the measured pH values to pC_{H+} have been measured for several electrolyte solutions of interest in waste tank chemistry.

In this approach solutions were prepared for titration that were as close as possible in bulk electrolyte concentration to the actual waste simulants yet did not include lesser concentration species, such as aluminate, which were predicted to precipitate at the starting pH values for the test solutions. The solutions were titrated using 3M NaOH since it was found in preliminary experiments that it was impossible to titrate solutions with high nitrite using acid owing to the formation of nitrous acid. All pH probes used during this study were Orion glass electrodes. The titrations were conducted starting at relatively low pH (~11) and NaOH added until the solution pH equaled 13 or the solution volume change was 5% of total volume (whichever condition was reached first).

The concentrations of the major electrolytes $NaNO_3$, $NaNO_2$, and Na_2CO_3 used in each titration along with the experimentally determined value of A are given in Table 4 for the different tank simulants as well as the A values for the single electrolyte solutions which serve as references. Also included are the experimental pH values for the tanks simulants and the calculated pC_{H+} values. In general the results show that the analytically determined pC_{H+} values in solutions with greater than 2M $NaNO_3$ are higher than the pH values whereas the solutions with lower $NaNO_3$ but higher carbonate follow the opposite trend. The single electrolyte $NaNO_3$ and Na_2CO_3 solutions also show a similar trend. A values increase with increasing $NaNO_3$ concentration but systematically lower when Na_2CO_3 is added to the $NaNO_3$ (see the constant 3M Na case in Table 4). Currently it is unknown if the corrosion potential of solutions is more positively correlated with the convention dependent pH or the analytically determinable pC_{H+} . However, determination of the pC_{H+}, or equivalently the free hydroxide concentration, at these lower base conditions would appear to be more consistent with the current approach of determining free hydroxide concentration analytically at higher base concentration.

Table 4: Experimentally determined difference between solution pH values in terms of activities and the analytically determined hydrogen ion concentrations. The value of A is defined in equation (1).

Simulant	**Electrolyte Components**	**Concentration**	**Experimental A Value**	**pH**	**pC_{H+}**	**Log Kw**
AY-101 Segment 3	$NaNO_3$	1.052	-0.40			
	$NaNO_2$	0.175		10.22	9.82	-13.64
	Na_2CO_3	0.588				
AY-101 Segment 8	$NaNO_3$	1.75	0.0			
	$NaNO_2$	1.08		12.51	12.51	-13.96
	Na_2CO_3	1.10				
AN-102	$NaNO_3$	3.108	0.62			
	$NaNO_2$	1.853		11.07	11.69	-14.4
	Na_2CO_3	1.103				
AY-102	$NaNO_3$	0.004	-0.27			
	$NaNO_2$	0.296		10.24	9.97	-13.44
	Na_2CO_3	0.405				
SY-102 (high Cl)	$NaNO_3$	2.048	0.18			
	$NaNO_2$	1.642		12.99	13.68	-14.18
	Na_2CO_3	1.05				
SY-102 (high NO_3)	$NaNO_3$	4.215	0.74			
	$NaNO_2$	0.112		9.9	10.64	-14.38
	Na_2CO_3	0.198				

Simple Electrolytes	Concentration	Experimental A Value	Log Kw
$NaNO_3$	1M	-0.10	-13.76
	3M	0.28	-14.09
	6M	1.1	-14.86
$NaNO_2$	1M	-0.25	-13.59
	3M	-0.08	-13.67
	6M	0.15	-13.97
Na_2CO_3	1M	-0.63	-13.30
Na_2SO_4	1M	-0.66	-13.28
2.8M $NaNO_3$+ 0.1M Na_2CO_3	3M Na	0.23	-14.06
2.4M $NaNO_3$+ 0.3M Na_2CO_3	3M Na	0.09	-13.96
2.0M $NaNO_3$+ 0.5M Na_2CO_3	3M Na	-0.05	-13.85

Summary

The overall objective of this research program was to determine the changes in supernatant or condensate chemistry that could occur on the surface of waste tank steels as the solutions dried and exchanged gases with the vapor phase and what potential impacts such changes could have on the corrosion of DST steels in the tank headspace. In order to achieve this objective required a knowledge of the most important vapor phase species that could impact tank steel corrosion as well as a coordinated chemical modeling and experimental approach to assess both the changes that could occur as the solutions dried and what impact such changes could have on steel corrosion. In this regard, it was found that although a wide range of vapor species have been identified in the DST's, the principal gas phase species likely to impact waste tank corrosion were CO_2 and NH_3 since these gases were present at much higher concentration than any other gases in the system and can act as either acids (CO_2) or bases (NH_3) as they exchange with tank condensates or supernatants. Different chemical models were tested to assess their range of reliability in modeling highly concentrated solutions resulting from supernatant evaporations. In general the mixed-solvent electrolyte (MSE) option in the ESP (OLI Systems) proved to be the most stable numerically for evaporation or drying problems. The results of the modeling calculations were also tested by conducting experiments of supernatant drying in contact with important vapor space gases (i.e. CO_2). In general the MSE option in ESP proved reliable in predicting both the changes in solution chemistry that occurred during supernatant evaporation as well as in predicting the solid phase precipitates that formed. The major exception occurred in systems that did not reach thermodynamic equilibrium, either because the solutions did not reach equilibrium with the gas phase or the thermodynamically stable solid phase did not form. In such cases ESP did not accurately predict the final solution phase compositions since it is an equilibrium thermodynamic model. However, in all cases examined the ESP model predictions showed lower pH values than actually measured either because the tank simulant evaporated before reaching equilibrium with the acidic CO_2 gas or Al containing phases, such as dawsonite, did not form in the system. The formation of the Al containing phases effectively would have removed hydroxide and lowered the resulting pH of the system. Hence the use of chemical models to predict the near surface chemical composition of evaporating supernatants appears to be justified if the results are interpreted as the worst possible case in terms of the solution pH value. Although very preliminary, the initial studies of tank steel corrosion using the equilibrated waste tank simulant compositions appears to follow the expected trends of greater corrosion rates at high nitrate concentration and lower pH. Methods were also presented for the determination of the actual solution phase hydrogen ion concentration, or equivalently the free base concentration, at lower pH values. The possible correlation of tank corrosion rates with the solution phase hydrogen ion concentration, rather than convention dependent pH measurements, has yet to be fully resolved.

Acknowledgements

The authors would like to especially thank Leon Stock for his invaluable advice and support during the course of this research program. A portion of the research was performed using EMSL, a national scientific user facility sponsored by the Department of Energy's Office of Biological and Environmental Research and located at Pacific Northwest National Laboratory.

References:

1. RPP-RPT-31129, 2006, Expert Panel Workshop on Double-Shell Tank Vapor Space Corrosion Testing, CH2M Hill Hanford Group, Inc., Richland, Washington.

2. Felmy A.R. and Qafoku O. (2007). Chemical Species in the Vapor Phase of Hanford Double-Shell Tanks: Phase 1: Available data and chemical modeling approach. Letter Report.

3. OLI Systems, Inc., The Environmental Simulation Program, Version 7.0.55, October 2, 2007.

4. Felmy A.R. and Qafoku O. (2008). Chemical Species in the Vapor Phase of Hanford Double-Shell Tanks: Phase 2: Implementation of the chemical modeling approach to predict changes in supernatant DST and vapor phase condensate compositions. Letter Report.

5. Felmy A.R. and Qafoku O. (2009) Development of Chemical Information for Vapor Space Corrosion Testing: Thermodynamic modeling of DST supernatant evaporations. Letter Report.

6. Mesmer R.E. (1991). Comments on 'A New Approach to Measuring the pH in Brinces and Other Concentrated Electrolytes' by K.G. Knauss, T.J. Wolery and K.J. Jackson. Geochimica et Cosmochima Acta. 55 (4), 1175-1176.

7. Rai D., A.R. Felmy, S.P. Juracich, and L. Rao (1995). Estimating the Hydrogen Ion Concentration in Concentrated NaCl and Na_2SO_4 Electrolytes. SAND94-1949. Sandia National Laboratories, Albuquerque NM.

8. Hoffman L. (2010). Corrosion Testing in Simulated Tank Solutions. SRNL-STI-2010-00509. Savannah River National Laboratory, Aiken SC.

Appendix A:

Gran titration procedure.

For the modified Gran titration procedure the electrolytes (Table 4) were titrated using 0.1, 1, and 3M NaOH depending on the electrolyte concentration. All pH probes used during this study were Orion glass electrodes. The titrations were terminated if solution pH reached 13 or the solution volume change was equal to 5% of total volume (whichever condition was attained first). The data collected during titrations (the measured pH and the volume of base added (mL)) were used to calculate the A value (see equation 1 and 3). Equations 1-3 are defined based on H+ ion concentration while the probe titration was conducted using hydroxide. This requires a rearrangement of these equations in terms of base concentration in order to analyze the probe titration data. From the apparent equilibrium constant of water the concentration of hydroxide ion and hydroxide observed ion:

$$C_{H}^{+} = K_w/C_{OH}^{-} \quad (4)$$

and,

$$H^{+}_{obs} = K_w/ OH^{-}_{obs} \quad (5)$$

where C_{OH}^{-} is the concentration of OH^- added (mol/L) during titration; H^{+}_{obs} is the observed reading with the calibrated pH electrode; K_w is apparent constant of water dissociation. After substitution of equation (4) and (5) into equation (3) yields,

$$K_w/OH^{-}_{obs} = 10^{A} K_w/C_{OH-} \quad (6)$$

rearranging and simplifying, yields

$$OH^{-}_{obs}/ C_{OH-} = 10^{-A} \quad (7)$$

Hence, a plot of C_{OH-} (mol/L) on the x-axes and $OH^{-}_{obs.}$ (mol/L) on y-axes yields a linear relationship. The logarithm of its slope is defined by the expression

$$A = -\log \text{slope} \quad (8)$$

It is worth mentioning that we often found curvature of the linear plot at the initial or end values of titration. The curvature at the initial point indicates consumption of hydroxide by minor aqueous species initial present in solution, while the curvature at the end point indicates that the higher hydroxide added has impacted the overall solution composition. Only the linear part was used for the fitting and slope calculation. Two examples of probe calibration graphs and their respective slopes and calculated A values are shown in the figures below:

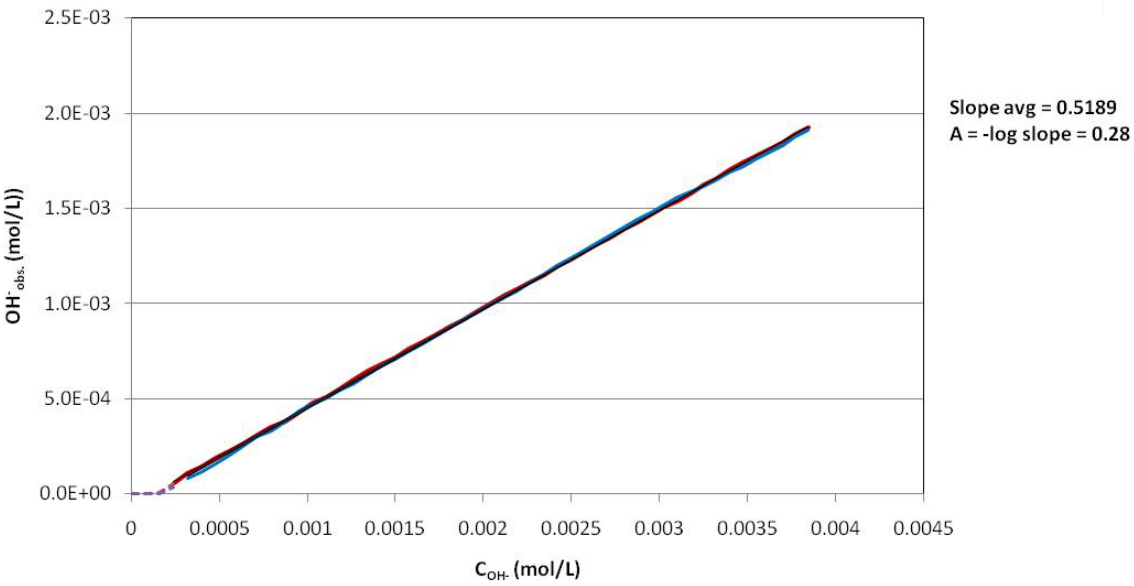

Figure A1. – probe calibration data for 3M $NaNO_3$ solution using 0.1M NaOH as titrant.

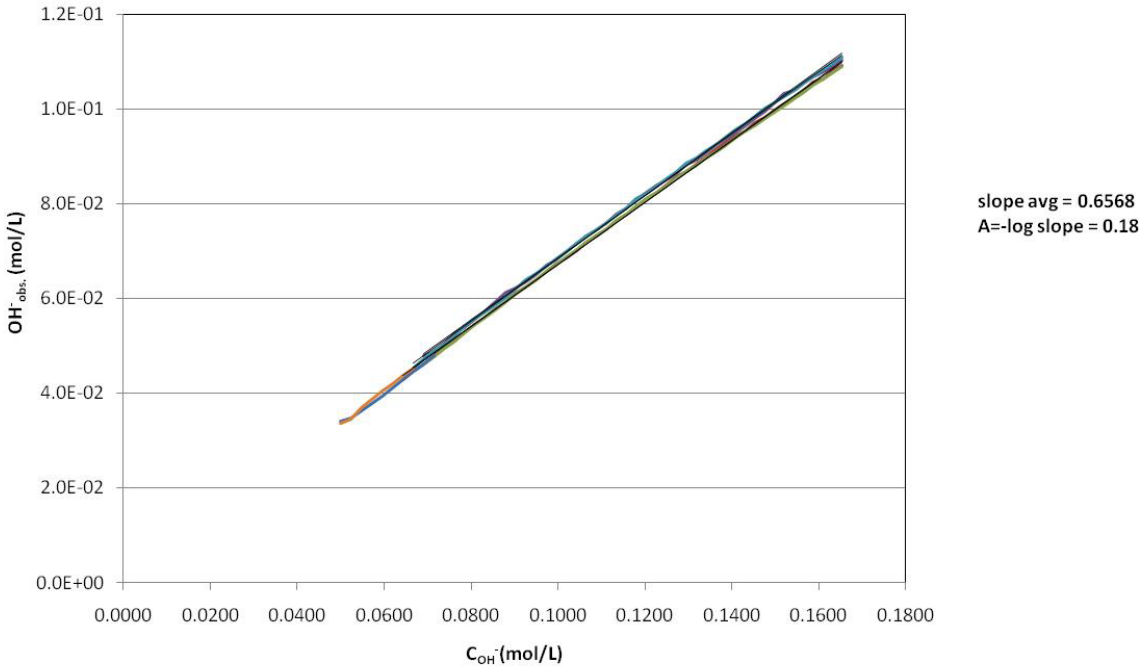

Figure A2. – probe calibration data for SY102 high Cl simulant using 3M NaOH as titrant.